An engineering model for the induction of crosswind kite power systems

Gaunaa, Mac; Meyer Forsting, Alexander; Trevisi, Filippo

Published in:
Journal of Physics: Conference Series

Link to article, DOI:
10.1088/1742-6596/1618/3/032010

Publication date:
2020

Document Version
Publisher's PDF, also known as Version of record

Journal of Physics: Conference Series

PAPER • **OPEN ACCESS**

An engineering model for the induction of crosswind kite power systems

To cite this article: Mac Gaunaa *et al* 2020 *J. Phys.: Conf. Ser.* **1618** 032010

An engineering model for the induction of crosswind kite power systems

Mac Gaunaa, Alexander Meyer Forsting, Filippo Trevisi

DTU, Department of Wind Energy, Frederiksborgvej 399, 4000 Roskilde, Denmark

macg@dtu.dk

Abstract. The present paper introduces a new, physically consistent definition of effective induction that should be used in engineering models for power kite performance that use aerodynamic coefficients for the wing. It is argued that in such cases it is physically inconsistent to use disc-based induction models – like momentum models – and thus a new, physically consistent induction model using vortex theory methodology is derived. Simulation results using the new induction model are compared to the previously often used momentum method and Actuator Line (AL) CFD simulations. The comparison shows that the new vortex based model is in much better agreement with the AL results than the momentum method. The new model is as computationally light as the momentum induction method.

1. Introduction

Theoretical and computational works [1-2] indicate that airborne wind energy systems, and in particular crosswind kites, have the potential to significantly decrease the cost of the highly needed sustainable and renewable energy. Therefore, the interest in this field has been steadily increasing. The fundamental power production potential using crosswind kites was given by Loyd [3]. This work showed that the ideal, obtainable power scales, as expected, with the cube of the onset wind speed - as for conventional wind turbines. Newer studies, such as for instance the work of Argatov et al. [4], showed that, in case there is a blockage effect the power scales with the cube of the reduced wind speed at the kite location. This signifies that the power reduction for relatively modest reductions of the effective wind speed at the kite location can still be significant. For instance, a 5% reduction of the wind speed will result in a power reduction of close to three times that value: $((1-5/100)^3-1)\cdot 100 = -14.3\%$.

It is well-known from the wind turbine community that the aerodynamic loading on the wings themselves can have a significant blockage effect on the effective wind speed at the wing. This self-induced blockage is conventionally termed "induced velocity". For a turbine operating at maximum power production, the axial wind speed in the rotor-plane is approximately 2/3 of the freestream value; so the induction factor in this case is a = 1/3. This can be shown with classic 1D momentum methods, which is a well validated and highly used workhorse in the wind turbine community [5]. The momentum based models are basically actuator disc models, where the underlying theory assumes the aerodynamic load to be distributed evenly in the azimuthal direction.

Since the power production potential of the crosswind kites strongly depends on the wind speed at the location of the kite, it is important to know the kite's self-induction. To the authors' knowledge, all previous engineering-type induction estimates have effectively been based on momentum-theory-based models, for instance [6-11]. References [6-10] used momentum-based modelling directly, whereas [11]

applied an engineering approximation to vortex cylinders [12]. In the steady case and for high kite speed ratios - corresponding to a high ratio between kite eigenvelocity and onset inflow velocity - the latter yield results identical to momentum theory [5,11]. Other studies have resorted to more computationally intensive CFD calculations [13-14] to quantify the effects of induction. However, in order for the results of these simulations to be analyzed, understood and used for subsequent engineering simulations, a consistent method for extracting physically meaningful induction from the data is needed.

When the solution of the same problem is analyzed with a vortex-based approach, which takes into account more of the details of the actual wake – so not relying on the disc assumption - the values of the effective induced velocities are generally significantly different than suggested by momentum-based models, as will be shown in this paper.

The objective of the present work is to use basic vortex theory building blocks to determine a new, physically consistent method for assessing the steady state induction of crosswind kites that can be applied in engineering models, where the baseline aerodynamic performance is given as baseline lift, drag and possibly moment coefficients for the kite. The performance and behavior of both the new vortex based model and the traditional momentum based type will be highlighted in the results section, where results from the engineering models are compared to each other, and to simulations from a higher fidelity CFD based actuator line model.

2. Methodology

At the absolute core of the present work is an accurate definition of what a physically consistent induction model should include. This is treated in subsection 2.1 below. According to the authors' knowledge, this is a novel contribution. After the framework has been defined, a new engineering induction model is formulated from vortex theory in section 2.2. The induction model uses the 3D aerodynamic polars of the kite, and is to the authors' knowledge also a new contribution to the field. The subsequent section states the well-known classic momentum-based model, with which the vortex based model will later be compared. Finally, the last subsection describes the high fidelity CFD Actuator Line (AL), which will be used as the numerical approximation of the true solution in the subsequent results section.

2.1. A physically consistent definition of induction

A physically consistent incorporation of induction in kite engineering models can be investigated by applying basic tools from vortex theory [5]. The Kutta-Joukowski theorem relates the forces on a flying wing to its bound circulation, and according to Kelvin's theorem for conservation of vorticity, changes in the bound circulation along the wing result in vorticity being trailed into the wake. As the Biot-Savart allows moving from a vortex system to a velocity field, this framework can be used to evaluate the induced velocities at any given location, when the magnitude and location of all vorticity is known.

When these tools are combined and applied to a high aspect ratio wing in straight translatory motion, it results in Prandtl's lifting line theory, which can be used to model - in a physically consistent way - the effect of three-dimensionality on a finite wing. One of the key results from this is that the induced drag coefficient scales with the lift coefficient squared and inversely with the wing aspect ratio. The induced drag is caused by an induced velocity opposite to the lift direction, due to the vorticity trailed from the wing. This effectively tilts the local lift vector backwards, which acts locally in the direction perpendicular to the local relative velocity. This causes the local lift to have a component in the global drag direction, thus giving rise to induced drag.

Therefore, when the aerodynamic performance is given for the kite (3D aerodynamic polars), the three-dimensionality of the aerodynamics is partially already included. In the lifting line case, the effect of the straight vortex system trailed after the wing is already included, and the effects of it are already imbedded in the 3D lift and drag coefficients. Care should therefore be taken when analyzing measured or calculated data to infer what the induced velocity is as "felt" by the kite. In fact, the definition of the angle of attack of a finite wing is the angle between the kite mid-span airfoil chord and the "undisturbed

reference wind" at the kite position. This is not a directly measurable flow angle anywhere close to the wing.

The novel idea of the present work is that this "undisturbed reference wind" can be found by subtracting from the total velocity field of any case the velocities induced by the vorticity system that the 3D polars correspond to. This idea can be considered a generalization, or adaptation, of the idea successfully used in [15] and [16] to determine the 2D angle of attack locally on wind turbine blades. In [15], the idea is used to infer 2D airfoil data from 3D calculations or measurements. In [16] the idea is used to develop a method to incorporate the effect of curved wind turbine blades. In both references, the induced velocities of the 2D sections are subtracted from the total 3D field to determine local effective conditions for the 2D sections. So the velocities induced from the corresponding vortex system for which we wish to use performance polars (2D) is subtracted from the full velocities to obtain the appropriate reference velocity and direction to be used in the 2D model.

With this in mind, the physically meaningful induction that should be used in cases where the aerodynamic data for the kite is based on 3D polars (from performance in classic straight translatory motion), is obtained by subtracting the inductions corresponding to that vortex system (standard translatory case) from the total inductions of the actual case; both velocities evaluated at the kite position. This way, it is ensured that each disturbance is included only once in the engineering modelling. If we use the same method to evaluate the classic translatory motion of the wing, we end up with zero induction. This is the correct result, because the velocities stemming from the disturbance of the kite itself is already included in the 3D polars.

With this knowledge, it is also evident that using momentum models to evaluate the self-induction for a kite that is described by 3D aerodynamic polars, is not physically consistent. The effect of the trailed vorticity from the straight-flying baseline case is already included in the 3D polars. An additional reason why using momentum models is dubious in the case of kites appear when examining the case where momentum models are highly successful: the wind turbine case. In this case, momentum models are used to take into account the presence of the rotor, as observed from a 2D section on the rotor. Since the inner two-dimensional aerodynamic model does not have any associated trailed vorticity, the use of the momentum model does not result in a "double counting" of any trailed vorticity. The momentum models are used in the wind turbine cases with a tip correction to (approximately) take into account that the rotor is not a disc, but has a finite number of wings. In fact, Prandtl's tip correction, which is normally used for wind turbines, is an approximation of the somewhat more complex Goldstein function [17], which can be used to take into account also the root-loss. Prandtl's function approximates the Goldstein function nicely for the usual wind turbine cases, where the tip speed ratios are not too low (usually TSR>6) and where the aerodynamically effective part of the blades extend almost to the rotation axis. For the kite case, there is (usually) only one "blade" circling in the "rotor-plane", and the effective "root" (inner kite tip) of the blade is often at 80%-90% of the radius of the "tip" (outer kite tip). In this case the Goldstein function would be immensely different from Prandtl's tip correction, and it would be an extremely large correction to the raw momentum results. This case is very far from the comfort zone of the methods used in the wind turbine community.

2.2. Vortex-based induction model

With the formal definition of induction as given in the previous subsection, it is now possible to uniquely determine an induction model which is appropriate for use in engineering models where the aerodynamic performance of the kite is determined using aerodynamic coefficients for the kite (as opposed to 2D airfoil coefficients). The aerodynamic performance includes lift, drag and possibly moment coefficients based on straight line motion, (for instance functions of kite angle of attack and possibly a yaw angle).

It is known from lifting line theory [5], that the ideal load shape for a straight wing in straight line motion is elliptic. This load shape minimizes induced drag. What can also be learned from lifting line theory is that deviations from the elliptic load shape do not result in drastically different performance: the key behaviour of any wing is close to that of the ideal, elliptically loaded wing. Induced drag coefficients scale with lift coefficient squared and inversely with aspect ratio, and lift curve slopes

decrease with aspect ratio. Therefore, the present induction model is based on the assumption that the circulation distribution of the kite is elliptic. For a wing with an elliptical bound circulation along the span

$$\Gamma = \Gamma_0\sqrt{1-\tilde{x}^2} \quad \text{where} \quad \tilde{x} = \frac{x}{S/2} \tag{1}$$

Here Γ is bound vortex strength, x is the spanwise coordinate with mid-span as origin and S is the wing span. From Helmholtz' law we find from this that the strength of the trailed vorticity sheet behind the wing is

$$\gamma(\tilde{x}) = \frac{\Gamma_0}{S/2}\frac{\tilde{x}}{\sqrt{1-\tilde{x}^2}} \tag{2}$$

From this expression the center of the trailed vorticity (corresponding to the center of gravity) for each side of the wing is

$$\tilde{x}_t = \pm\frac{x}{S/2} = \pm\frac{\int_0^{S/2} x\,\gamma dx}{S/2\int_0^{S/2}\gamma dx} = \pm\frac{\int_0^1 \frac{\tilde{x}^2}{\sqrt{1-\tilde{x}^2}}dx}{\int_0^1 \frac{\tilde{x}}{\sqrt{1-\tilde{x}^2}}dx} = \pm\frac{\pi}{4} \tag{3}$$

It is therefore assumed that the distance between the rolled up tip-vortices in the wake further behind the wing will be $\Delta = \frac{S}{2}\left(\frac{\pi}{4}+\frac{\pi}{4}\right) = S\frac{\pi}{4}$. A numerical time stepping evaluation of the development of the initially straight cross-section of the vortex sheet after the wing was implemented, and the results showed that the distance between the rolled-up center of trailed vorticity from the two halves of the wing matched very accurately the analytical results from Eq.(3). The magnitude of the circulation of each tip vortex is $\int_0^{S/2}\gamma\,dx = \Gamma_0$, but with opposite signs. Therefore the self-induced velocity of the rolled-up tip vortex pair can be estimated assuming that they act roughly as 2D vortices:

$$V_{tip,self} = \frac{\Gamma_0}{2\pi\Delta} = \frac{2\Gamma_0}{\pi^2 S} \tag{4}$$

Joukowski's equation, $\vec{f} = \rho\overrightarrow{V_R}\times\vec{\Gamma}$, can be used to link the local force per spanlength, $\vec{f}$, to density, ρ, local bound circulation, $\vec{\Gamma}$, and local relative velocity (excluding the part induced by the bound vortex itself), $\overrightarrow{V_R}$. The wing mid-span trajectory is assumed to be circular with radius R, the circle path lies in a plane perpendicular to the undisturbed onset flow with velocity $V_{\infty R}$. The wing span direction is purely radial: so the relative flow velocity from the onset flow and wing motion are perpendicular to the wing.

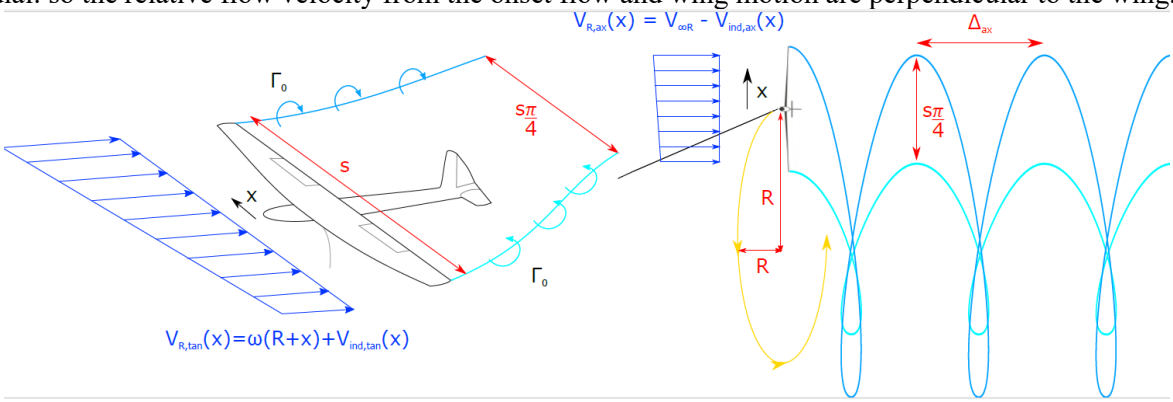

Figure 1: *Inflow velocity to the kite are split up into components in the axial and tangential directions, respectively. The distance between the rolled up tip vorices behind the wing of spanlength S is Sπ/4, and the distance between subsequent passes of the helical trailed vortices is Δ_{ax}.*

Figure 1 show a representation of the key properties used in the derivation of the present model. The derivation of the basic induction model is done in a reference system with no axial velocity of the kite (=reel out velocity in the case of ground-gen system), because the effect of this can be easily introduced later by use of a shift of the coordinate system. The velocity relative to the wing in the axial direction is $V_{R,ax}(\tilde{x}) = V_{\infty R} - V_{ind,ax}(\tilde{x})$ and $V_{R,tan}(\tilde{x}) = \omega(R+x) + V_{ind,tan}(\tilde{x}) = V_k + V_k\frac{S}{R}\frac{\tilde{x}}{2} + V_{ind,tan}(\tilde{x})$ in the tangential direction. $V_k = \omega R$ is the eigen-velocity of the kite. Note that the induced velocities in

these expressions are the full induced velocities from the whole system of trailed vorticity. If these induced velocities are assumed to vary linearly over the spanlength, it is seen from integration of Joukowski's equation, that the integral forces in the axial and tangential directions depend only on the mid-span magnitudes of the relative velocity ($V_{ind,0,ax}$ and $V_{ind,0,tan}$), and not on the slopes of the relative velocities: $F = \int_{-S/2}^{S/2} f\, dx = \frac{S}{2}\rho\Gamma_0 \int_{-1}^{1}(V_m - V_m{}'\tilde{x})\sqrt{1-\tilde{x}^2}d\tilde{x} = \frac{\pi}{4}\rho S\Gamma_0 V_m$. From this we get that the integral forces in the axial and tangential directions from the bound vorticity turns out to be:

$$F_{ax} = \frac{\pi}{4}\rho S\Gamma_0\left(V_k + V_{ind,0,tan}\right) = \frac{\pi}{4}\rho V_{\infty R} S\Gamma_0(\widetilde{V_k} + V_{ind,0,tan}/V_{\infty R}) \approx \frac{\pi}{4}\rho V_{\infty R} S\Gamma_0 \widetilde{V_k} \quad (5)$$

$$F_{tang} = \frac{\pi}{4}\rho S\Gamma_0\left(V_{\infty R} - V_{ind,0,ax}\right) = \frac{\pi}{4}\rho V_{\infty R} S\Gamma_0\left(1 - V_{ind,0,ax}/V_{\infty R}\right) \quad (6)$$

Here the non-dimensional variable $\widetilde{V_k} = V_k/V_{\infty R}$ has been introduced for the relative kite velocity. The last approximation for the axial force is usually very good, because generally $\widetilde{V_k}$ is in the order between 5 to 10, and therefore much larger than the tangential induced velocity.

If we turn now to the classical nonrotating case, we can get from integration of the half-infinite trailed vorticity sheet inductions, using Eq. (2), that the induced velocities in the classical straight motion wing case has the constant value

$$V_{i,LL} = \int dV_i = \int_{-S/2}^{S/2} \frac{\gamma\, dx_v}{4\pi(x - x_v)} = \frac{\Gamma_0}{2\pi S}\int_{-1}^{1} \frac{\widetilde{x_v}}{(\tilde{x} - \widetilde{x_v})\sqrt{1 - \widetilde{x_v}^2}} d\widetilde{x_v} = \frac{\Gamma_0}{2S} \quad (7)$$

Joukowski's equation can be employed as previously to find the integral lift and induced drgag forces as $L = \int_{-S/2}^{S/2} \rho V_R \Gamma \mathrm{dx} = \frac{\pi}{4}\rho V_R S\Gamma_0$ and $D_i = \int_{-S/2}^{S/2} \rho V_{i,LL}\Gamma \mathrm{dx} = \frac{\pi}{4}\rho V_{i,LL} S\Gamma_0 = \frac{\pi}{8}\rho {\Gamma_0}^2$

Upon noting that the definition of aspect ratio is $AR = S^2/A$, where A is the wing planform area, we can now finally obtain a general relation between the lift coefficient and the mid-span bound circulation strength Γ_0:

$$C_L = \frac{L}{\frac{1}{2}\rho V_R^2 A} = \frac{\frac{\pi}{4}\rho V_R S\Gamma_0}{\frac{1}{2}\rho V_R^2 A} = \frac{\pi\Gamma_0 AR}{2V_R S} \quad \Leftrightarrow \quad \Gamma_0 = \frac{2V_R S C_L}{\pi AR} \quad (8)$$

If this is inserted in the previous expression for the induced drag, we get the classical lifting line result $C_{Di} = \frac{\pi}{8}\rho {\Gamma_0}^2/(0.5\rho V_R^2 A) = C_L^2/(\pi AR)$. Additionally, since the induced velocities in this case are constant $C_{Di} = C_L\alpha_i$, so the classic induced angle of attack in the straight motion wing case turns out to be $\alpha_i = C_L/(\pi AR) = \Gamma_0/(2V_R S)$.

In the circling wing case a good approximation is $V_R \approx V_{\infty R}\widetilde{V_k}$, so we finally get

$$\Gamma_0 = \frac{2V_{\infty R}\widetilde{V_k} S C_L}{\pi AR} \quad (9)$$

This relation is the link between lift coefficient and mid span circulation for the circling wing case. If Eq. (9) is combined with Eq. (5) and Eq. (6) we get

$$F_{ax} \approx \frac{1}{2}\rho\left(V_{\infty R}\widetilde{V_k}\right)^2 \frac{S^2}{AR} C_L = \frac{1}{2}\rho\left(V_{\infty R}\widetilde{V_k}\right)^2 A C_L = L \quad (10)$$

$$F_{tang} = \frac{F_{ax}}{\widetilde{V_k}}\left(1 - V_{ind,0,ax}/V_{\infty R}\right) = \frac{L}{\widetilde{V_k}}\left(1 - V_{ind,0,ax}/V_{\infty R}\right) \quad (11)$$

The result in Eq. (10) is the expected case under the used assumption of a high relative velocity of the wing to the onset flow. The result in Eq. (11) can be more easily understood by writing $V_{ind,0,ax} = V_{i,LL} + V_{ind,eff}$, where $V_{ind,eff} = V_{ind,0,ax} - V_{i,LL}$ is seen to be exactly the axial component of the induced velocity as defined in section 2.1. Inserting the latter expression into Eq. (11), while noting that $V_{i,LL}/\left(V_{\infty R}\widetilde{V_k}\right) = V_{i,LL}/V_R = \alpha_i = D_i/L$ the following equation is obtained

$$F_{tang} = L\frac{V_{\infty R} - V_{ind,eff}}{V_{\infty R}\widetilde{V_k}} - L\frac{V_{i,LL}}{V_{\infty R}\widetilde{V_k}} = L\frac{V_{\infty R} - V_{ind,eff}}{V_{\infty R}\widetilde{V_k}} - D_i \quad (12)$$

The term $(V_{\infty R} - V_{ind,eff})/\left(V_{\infty R}\widetilde{V_k}\right)$ can be interpreted as $\tan(\theta_{rel})$, where θ_{rel} is the tilt back of the relative wind vector due to the effective axial flow velocity $V_{\infty R} - V_{ind,eff}$. If the approximation of $V_R \approx V_{\infty R}\widetilde{V_k}$ had not been used, the equation would have read $F_{tang} = L\, sin(\theta_{rel}) - D_i cos(\theta_{rel})$. This shows mathematically the main take-away from Section 2.1: the correct way to use tabulated data (which

in the lifting line case is exactly L and D_i) for a finite wing is to use an effective induction, which is the total induced velocity from the total vortex system minus the inductions from the corresponding straight translatory, flat wake case:

$$V_{ind,eff} = V_{ind,0,ax} - V_{i,LL} \tag{13}$$

Far wake model

The tools derived above can now be used to appropriately model the effective induction. The first model captures the difference between the vortex systems of the actual and the translatory case corresponding to the wake from half a rotation away to infinity. In this region, it is assumed that the sheet has had time to roll up into distinct tip vortices. Numerical investigations of this vortex system have shown that the effective induction is very close to constant along the span in this case. Also, the induction from the flat translatory counterpart of the wake is very small, because these start approximately $\Delta l_{1/2}/S = \pi R/S$ away, which for realistic cases of flight radius and spanlength result in vanishingly small inductions from the translatory vortex system. This means that effectively, the far wake model for the induced velocity stems from the tip vortices organized in a helical structure downstream. A numerical implementation of such a helical system (period length along the axial direction $\Delta l \approx 2\pi R/\tilde{V}_k$, tip vortex spacing $\Delta = S\frac{\pi}{4}$) was made, and inductions were compared with the much simpler 2D case with the same tip vortex spacing having the tip vortex pairs located at $(x, y) = (\pm S\pi/8, N \cdot \Delta l)$ where $N = 1..\infty$. The evaluation point is mid span, which in the 2D setting correspond to (x,y)=(0,0). Comparison of the (axial) inductions from these two models showed, that the induction from the simpler model using the 2D vortices was within 5% of the helical model for $\tilde{V}_k = [4 - 15]$ and $S/R = [0.01 - 0.2]$. Based on these results, the far wake model is built off the 2D vortex system. This has the added convenience that the mid-span induction can be calculated using the closed form solution for the induction of an infinite row of vortices (cascade vortex element [18]). Under the assumption that the dominant effect in the motion of the tip vortices through the surrounding fluid is the mutual interaction described in Eq. (4), the convection velocity of the tip vortices are

$$V_{conv} = V_{\infty R} - \frac{2\Gamma_0}{\pi^2 S} = V_{\infty R}\left(1 - \frac{4\widetilde{V_k}C_L}{\pi^3 AR}\right) \tag{14}$$

Therefore, the axial spacing of the tip vortex pairs turns out to be

$$\Delta_{ax} = \Delta t\, V_{conv} = \frac{2\pi R}{V_{\infty R}\widetilde{V_k}} V_{\infty R}\left(1 - \frac{4\widetilde{V_k}C_L}{\pi^3 AR}\right) = \frac{2\pi R}{\widetilde{V_k}}\left(1 - \frac{4\widetilde{V_k}C_L}{\pi^3 AR}\right) \tag{15}$$

This can be used together with the previously determined radial distance between the tip vortices, $\Delta = S\frac{\pi}{4}$, and the tip vortex strengths, $\pm\Gamma_0$ (with Γ_0 given from Eq. (9)) to determine the mid-span axial induction using cascade vortex elements. Symmetry conditions can be used to see that the axial induction of the vortex system in question is equal to the axial induction of one infinite row of 2D vortices minus the axial induction of one tip vortex at the tip of the span. After linearizing the result, the final version of the far wake induction turns out to be

$$\frac{V_{ind,far}}{V_{\infty R}} = \frac{\widetilde{V_k}^3\left(\frac{S}{R}\right)^2 C_L}{96\,\pi\, AR\left(1 - \frac{4\,C_L\widetilde{V_k}}{\pi^3 AR}\right)^2} \tag{16}$$

The positive direction for $V_{ind,far}$ is in the direction opposite to $V_{\infty R}$.

Near wake model

When investigating the induction of the near part of the vortex wake, i.e. the helical wake of the first half wake rotation, the main trend from the effective wake induction (helical wake induction minus the corresponding plane wake induction) is that there is now an almost constant gradient of the induction along the span of the blade. For a given S, the gradient of the induction scales linearly with S/R, such that constant induction along the span is approached when R is increased. However, it was shown above that the gradient of the inductions has no effect on the integral forces, and that only the mid-span induced velocities influence these if the variation in induction is linear. Investigations of the mid-span effective axial induction due to the first half of the wake vorticity (distributed wake sheet) showed only a very

small effective axial induction, corresponding to a seemingly small fraction of the far wake model values. Analysis of the mid-span effective near wake induction showed that for a given S and Γ_0, the mid span induction scaled with $(S/R)^2$. As will be evident from the results later, the far wake model alone does not provide a satisfactory agreement between the engineering model and the AL model for all calculated cases. The calculated values of the induction from the near wake part of the effective vortex wake only changed this insignificantly, which to the authors was very surprising. However, the basic knowledge from the vortex wake analysis above was used to propose an engineering approximation to the near wake induction, with only one parameter to be fitted according to the AL results. The basic idea is that the near wake induction should scale with $(S/R)^2$ and also with the flat wake induction, which from a combination of Eq. (7) and Eq. (9) turns out to be

$$V_{i,LL} = \frac{V_{\infty R}\widetilde{V_k}C_L}{\pi AR} \tag{17}$$

The suggested form of the near wake model is therefore

$$\frac{V_{ind,near}}{V_{\infty R}} = K_{far}\frac{\widetilde{V_k}\,C_L\left(\frac{S}{R}\right)^2}{AR} \tag{18}$$

Manual fitting of K_{far} against the AL data resulted in $K_{far} = 2$. The positive direction for $V_{ind,far}$ is, as for the far wake model, in the direction opposite to $V_{\infty R}$.

Total effective axial induction model

The final total model for the effective axial induction is the sum of the near and far wake models, Eqs. (16) and (18), with $K_{far} = 2$:

$$\frac{V_{ind,eff}}{V_{\infty R}} = \frac{\widetilde{V_k}^3\left(\frac{S}{R}\right)^2 C_L}{96\,\pi\,AR\left(1-\frac{4\,C_L\widetilde{V_k}}{\pi^3 AR}\right)^2} + 2\frac{\widetilde{V_k}\,C_L\left(\frac{S}{R}\right)^2}{AR} = \frac{\widetilde{V_k}\,C_L\left(\frac{S}{R}\right)^2}{\pi AR}\left(\frac{\widetilde{V_k}^2}{96\left(1-\frac{4C_L\widetilde{V_k}}{\pi^3 AR}\right)^2} + 2\pi\right) \tag{19}$$

The positive direction for $V_{ind,eff}$ is in the direction opposite to $V_{\infty R}$, such that the total effective axial velocity is $V_{\infty R} - V_{ind,eff}$.

Engineering model for elliptic translatory wing aerodynamic coefficients

An approximate value for the elliptic wing lift curve slope from lifting line theory is [5] $C_l'\frac{AR}{2+AR}$, where C_l' is the 2D lift curve slope. Therefore, for an untwisted elliptic wing of elliptic planform, the integral lift coefficient is

$$C_L = C_l'(\alpha - \alpha_0)\frac{AR}{2+AR} \tag{20}$$

According to the results derived in the sections above, there will be an induced drag. In addition to this, a real wing experiences drag due to viscous effects. As long as the flow remains attached, these can be assumed fairly constant. If the 2D profile drag coefficient is C_{dv}, then the viscous contribution to the wing drag coefficient will have the same value. Therefore, the wing drag coefficient will be

$$C_D = C_{dv} + \frac{C_L^2}{\pi\,AR} \tag{21}$$

2.3. Momentum-based model

To be able to cope with cases with high thrust coefficients, the baseline momentum model is extended with the widely used Spera model for high inductions [5]. The result is

$$\frac{V_{ind,mom}}{V_{\infty R}} = \begin{cases} \frac{1}{2} - \frac{1}{2}\sqrt{1-C_T} & if\ C_T \le {C_T}^* \\ \frac{\frac{C_T}{4} - 4a_c^2}{1-2a_c} & if\ C_T > {C_T}^* \end{cases} \tag{22}$$

$$C_T = \frac{F_{axial}}{0.5\rho {V_{\infty R}}^2 A_{swept}} = \frac{F_{axial}}{\pi\rho {V_{\infty R}}^2 RS} \tag{23}$$

In the model $C_T{}^* = 4a_c(1 - a_c)$, where a_c defines the induction factor limit from which C_T go from following the classical 1D momentum results, to the linear high induction correction zone. In the present work the value $a_c = 1/3$ has been used for the model coefficient.

2.4. Actuator line method

The actuator line model, unlike the actuator disc, captures transient physical features like shed and trailed vorticity (including root/tip vortices, and distinct blades) by distributing the blade forces - computed from 2D airfoil polars - in the flow domain. It employs a three-dimensional Gaussian force projection, following the original formulation of Sørensen and Shen [19]. The smearing length scale is twice the grid size as recommended by Troldborg [20] to guarantee numerical stability. The force smearing leads to over-predictions in the blade forces, which is counteracted by the correction of Meyer Forsting *et al.* [21].

To ensure that the outer wing tip remains within a single cell during one time step $\Delta t<\Delta x/(\omega R_{tip})$ - with mesh spacing Δx, radius from the center of the circular kite path to the outer tip R_{tip} and rotational speed of the kite motion ω.

The numerical domain for the kite simulations is discretized in a verified, standard manner [22, 20]. It consists of a box with 25R side length that contains an inner box with a uniformly spaced refined mesh of R+S edge length at its center surrounding the rotor. The mesh spacing in this region is Δx=S/20 and 30 uniformly spaced control points are employed along the kite span. The boundaries off the main flow direction are of the symmetry type, whereas the inflow and outflow faces obey Dirichlet and Neumann conditions, respectively.

3. Results

Initial translatory AL simulations

In order to assess the basic performance of the AL solver, elliptic planform wings were simulated. Elliptic planform planar straight wings are considered. The 2D airfoil performance used is is: $C_l' = 2\pi$, $\alpha_0 = 0$ and Cdv=0.01. Comparison between the AD simulations agreed very well with the performance (C_L and C_D) evaluated with the lifting line method, Eqs. (20) and (21). The difference in C_L for a given angle of attack was below 3.5% for angles of attack below 16°. Similarly, the difference in C_D was below 3% for all translatory simulations. This indicates that the AL calculations are set up correctly, and that using the lifting line engineering aerodynamic dataset in the engineering modeling below is feasible.

Elliptic planform wings in circular trajectories

The test cases from which the engineering model performances should be evaluated are set up to make a direct comparison relatively easy. For a real case kite, the kite relative speed is determined from equilibrium between the kite aerodynamic performance and the effective tether forces in the tangential direction. Running simulations of this type of setup would complicate the AL calculations significantly. Therefore, the models are tested in a different manner. The setup is kept simple by specifying a range of inputs that define the shape, path radius, spanlength and relative speed of the kite. This allows for a methodic comparison of the key output: Integral axial and tangential forces. The effect of the kite tether is not included here, as the modeling of this would be identical in the AL and engineering models.

Aspect ratio AR=[6, 12, 24]. $\widetilde{V_k}=V_k/V_{\infty R}$ is in the range between 5 and 15 (AL results for 5, 10 and 15). S/R in the range from 0.02 to 0.2 (AL results for 1/15=0.0667, 0.1 and 0.2). S is spanlength, R is distance from rotation axis to kite mid-span. The angle of the local chord-line to the rotation plane is oriented such that the no-induction case would run at an angle of attack of α_{noind} at mid-span. The majority of AL simulations use $\alpha_{noind} = 16^o$, but a few calculations are run for $\alpha_{noind} = 8^o$.

The engineering models require an iteration loop to calculate the integral forces in the axial and tangential directions. Initially, the effective induction is set to zero, after which the convergence loop is started. First relative velocity magnitude and angle of attack are determined. This allows for determination of the airfoil force coefficients, which allow for determination of the effective inductions. This sequence is repeated until the results have converged, which is usually very fast.

Below, Figure 2 shows a comparison between the results from the new vortex-based induction model and the classic momentum-based induction model. The results in the figure show that there can be a quite large difference between the induced velocities from the two different methods and that the methods have different relative sensitivities to changes in different quantities. The right plot shows that the relative differences between the two models seem to be roughly constant for a given S/R and $\widetilde{V_k} = V_k/V_{\infty R}$.

Figure 3 shows the axial forces (left) and tangential forces (right) predicted with the different methods for different relative kite speed (x-axis) and relative turning radii (*S/R*) for $\alpha_{noind} = 16^o$. AR=[6, 12, 24] results are shown in thick, intermediate and thin lines/markers, respectively.

Generally, the models agree to a higher degree on the axial forces, and the model differences become more apparent on the tangential forces, as expected. It is noted that the tangential force drops below zero for higher kite relative velocities for AR=6. This is caused by the high induced drag in those cases, which follows from the relatively high angle of attack combined with the low aspect ratio. The higher aspect ratio case does not have negative tangential forces anywhere in the investigated domain. The sign of the tangential force, however, is less important here, because the objective is to compare the results from the different models. Generally, it is seen that the vortex induction model results lie significantly closer to the AL results (regarded as being closest to the true result) than the

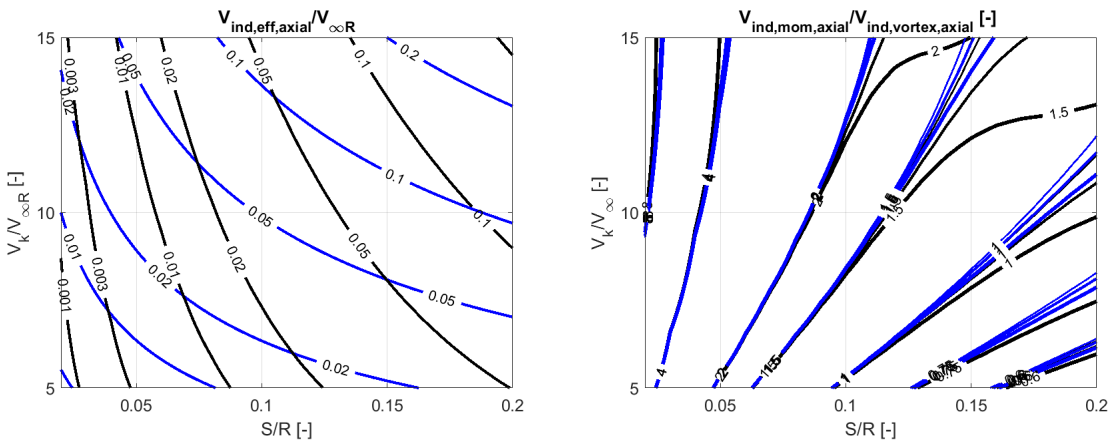

Figure 2: *Comparison between induced velocities from the classic momentum model and the new vortex based model. Wing planform is elliptic. Both plots show iso curves of different quantities as function of S/R and $V_k/V_{\infty R}$. Left: effective axial inductions for a AR=12 wing at $\alpha_{noind} = 16^o$. Blue: momentum results, Black: New vortex model. Right: Iso curves of the ratio between axial inductions from momentum and vortex methods. Thick/Intermediate/Thin curves signify AR=[6, 12, 24], Blue/Black signify $\alpha_{noind} = [8^o, 16^o]$.*

momentum induction results. Specifically, it is seen that the mometum model severely underpredicts the tangential force for the high relative kite velocities; especially for S/R=0.1 and 0.0667. This is caused by too large inductions predicted by the model. These differences were also apparent on Figure 2.

A comparison analog to those in Figure 3 has been made with a lower loading, for $\alpha_{noind} = 8^o$ and $S/R = 0.2$. The relative trends and agreement followed those presented in Figure 3.

4. Conclusions

One major finding in the present work is that the definition of physically meaningful induced velocities to use in an engineering model of kite performance is linked to the aerodynamic dataset used in the engineering model. This is a novel contribution of the present work.

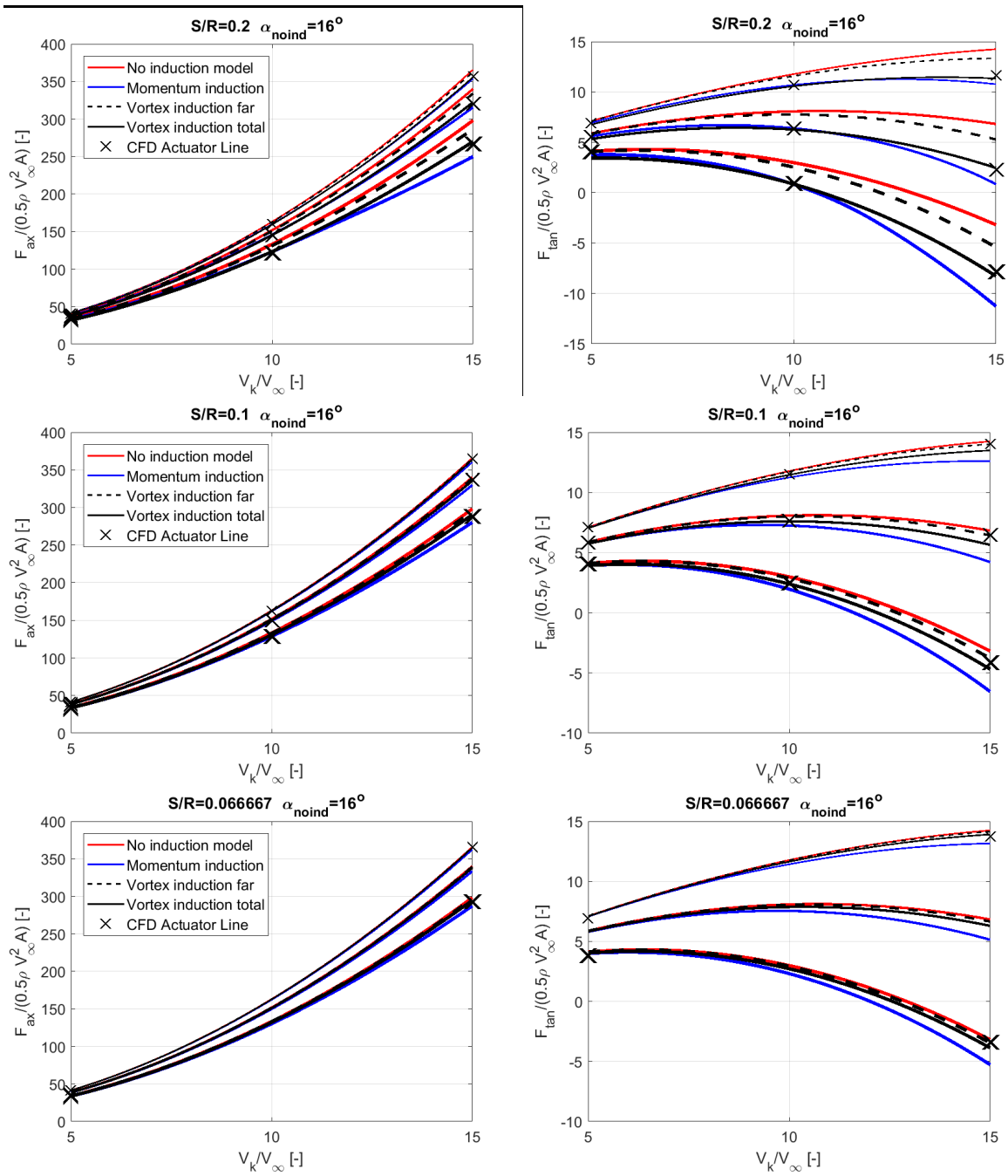

Figure 3: *Comparison of the performance of engineering models (momentum model and vortex models) with results from AL. Axial forces (left column) and tangential forces (right column) on elliptic wings moving in circular trajectories. Upper figures show results for S/R=0.2 ("small loop" radius), middle for S/R=0.1 ("intermediate loop" radius), and the lower for S/R=1/15=0.0667 ("large loop" radius). The results for elliptic planform wings of aspect ratios AR=[6, 12, 24] are shown in thick, intermediate and thin lines/markers, respectively. Results are shown as a function of kite velocity ratio.* $\alpha_{noind} = 16^o$

The present paper introduces a new, physically consistent definition of effective induction that should be used in engineering models evaluating the performance of power-producing kites that use aerodynamic coefficients for the wing. Based on this, it is argued and later shown using the vortex theory foundation, that it is physically inconsistent to use disc-based induction models such as momentum models in these cases. The basic reason for this is that a part of the effect of the vorticity is already included/embedded in the wing's aerodynamic performance.

A vortex theory based, physically consistent induction model has been derived. The model is designed for use in engineering models where aerodynamic coefficients is used for the kite. This is another novel contribution of this work.

Evaluation of the inductions with the physically consistent model from the present work are often very different from those obtained using momentum theory.

Simulation results using the new induction model are compared to the previously often used momentum method and Actuator Line (AL) CFD simulations. The comparison show that the new vortex based model is in much better agreement with the AL results than the momentum method. The computational complexity of the new model is of the same order as the momentum induction method.

5. Further work

- Understanding the reason for the inability of the vortex analysis method to determine the magnitude of the scaling factor in the near wake induction model.
- Investigation of the effects of varying relative inflow speed and direction on the bound circulation: how sensitive are the results to changes in the bound vorticity shape?
- How sensitive are these results to planform shape? (Rectangular wings?)
- How sensitive are the results to changes in the wing direction? Roll angle, yaw angle?
- Look into differences in losses in power due to the effective induced axial velocities for ground-gen and fly-gen kite systems
- Extension to unsteady modelling?
- Effects of multiple kites in the same circular path? If the splitting of the effective induction, and its modeling is correct in this model, the additional effective induced velocity would show in the far wake model only. Since this accounts for a small part of the total induction, the penalty of multiple kites in the same flight path might not be so big
- Investigate whether the induction from nearby flying kites can be determined using vortex cylinders [12]?
- Investigate whether operation in the wakes of other kites can be simulated using the DWM method [23].

References

[1] Heilmann J., Houle C. (2013) Economics of pumping kite generators. In: Ahrens U., Diehl M., Schmehl R. (eds) Airborne Wind Energy. Green Energy and Technology. Springer, Berlin, Heidelberg.

[2] Cherubini, A., Papini, A., Vertechy, R., Fontana, M. (2015) Airborne Wind Energy Systems: A review of the technologies. Renewable and Sustainable Energy Reviews, Volume 51, Pages 1461-1476

[3] Loyd, M.L. (1980). Crosswind kite power. Journal of Energy, 4(3), 106–111.

[4] Argatov I., Rautakorpi P., and Silvennoinen R. Apparent wind load effects on the tether of a kitepower generator. Journal of Wind Engineering and Industrial Aerodynamics, 2011.

[5] Branlard. E. (2017). Wind Turbine Aerodynamics and Vorticity-Based Methods. Textbook, Springer.

[6] Zanon, M., Gros, S., Meyers, J., and Diehl, M. (2014).Airborne wind energy: Airfoil-airmass

interaction. In Proceedings of the 19th World Congress The International Federation of Automatic Control. Cape Town, South Africa.
[7] Leuthold, R & Gros, S & Diehl, M. (2017). Induction in Optimal Control of Multiple-Kite Airborne Wind Energy Systems. IFAC-Papers On Line. 50. 153-158.
[8] Kheiri, M., Bourgault, F., Saberi Nasrabad, V. Victor, S.: On the aerodynamic performance of crosswind power systems. Journal of Wind Engineering & Industrial Aerodynamics 181 (2018) 1–13.
[9] Kheiri, m., Nasrabad, V.S., Bourgault, F. A new perspective on the aerodynamic performance and power limit of crosswind kite systems. Journal of Wind Engineering & Industrial Aerodynamics, 190 (2019) 190–199
[10] Lellis, M.D., Reginatto, R., Saraiva, R, Trofino, A. The Betz limit applied to Airborne Wind Energy. Renewable Energy 127 (2018) 32-40
[11] Leuthold, R., Crawford, C., Gros, S., Diehl, M. Engineering Wake Induction Model For Axisymmetric Multi-Kite Systems. IOP Conf. Series: Journal of Physics: Conf. Series 1256 (2019) 012009 IOP Publishing.
[12] Branlard, E., & Gaunaa, M. (2015). Cylindrical vortex wake model: right cylinder. Wind Energy, 18(11), 1973–1987.
[13] Kheiri, M., Bourgault, F., Saberi Nasrabad, V.: Power Limit for Crosswind Kite Systems. In Proceedings of ISWTP 2017, Montreal, Canada, May 2017.
[14] Haas, T., Meyers, J. Comparison study between wind turbine and power kite wakes. IOP Conf. Series: Journal of Physics: Conf. Series 854 (2017) 012019
[15] Shen, W. Z., Hansen, M. O. L., & Sørensen, J. N. (2009). Determination of the angle of attack on rotor blades. Wind Energy, 12(1), 91-98.
[16] Li, A., Gaunaa, M., Pirrung, G.R., Ramos-Garcia, N., Horcas, S.G., The influence of the bound vortex on the aerodynamics of curved wind turbine blades. submitted to TORQUE 2020.
[17] Sørensen, J.N., General Momentum Theory for Horizontal Axis Wind Turbines. Springer. 2016.
[18] Lewis, R.I., Vortex Element Methods for Fluid Dynamics Analysis of Engineering Systems. Cambridge University Press, 1991. ISBN 0 521 36010 2 hardback.
[19] Sørensen, J.N., Shen, W.Z., Numerical modelling of wind turbine wakes. Journal of Fluids Engineering 124(2):393-399. Jan 2002.
[20] Troldborg, N., Actuator Line Modeling of Wind Turbine Wakes. PhD Thesis, Technical University of Denmark. 2009.
[21] Meyer Forsting, A., Pirrung, G., & Ramos García, N. (2019). A vortex-based tip/smearing correction for the actuator line. Wind Energy Science, 4, 369-383.
[22] Meyer Forsting, A. Modelling Wind Turbine Inflow: The Induction Zone. PhD Thesis, Technical University of Denmark. 2017.
[23] Keck et.al., (2013). Two improvements to the dynamic wake meandering model: including the effects of atmospheric shear on wake turbulence and incorporating turbulence build-up in a row of wind turbines. Wind Energy, 18(1), 111–132.